

Published in final edited form as:

Adv Mater. 2020 May 01; 32(19): e1906889. doi:10.1002/adma.201906889.

Retrieving the co-assembly pathway of composite cellulose nanocrystal photonic films from their angular optical response

Dr Bruno Frka-Petecic*,

Melville Laboratory for Polymer Synthesis, Department of Chemistry, University of Cambridge, Lensfield Road, Cambridge CB2 1EW, United Kingdom

Dr Joel A. Kelly

Department of Chemistry, University of British Columbia, 2036 Main Mall, Vancouver, BC, Canada, V6T 1Z1

Gianni Jacucci, Dr Giulia Guidetti, Dr Gen Kamita, Nathan P. Crossette

Melville Laboratory for Polymer Synthesis, Department of Chemistry, University of Cambridge, Lensfield Road, Cambridge CB2 1EW, United Kingdom

Dr Wadood Y. Hamad,

Transformation and Interfaces Group, FPIInnovations, 2665 East Mall, Vancouver, BC, Canada V6T 1Z4

Prof Mark J. MacLachlan,

Department of Chemistry, University of British Columbia, 2036 Main Mall, Vancouver, BC, Canada, V6T 1Z1

Dr Silvia Vignolini*

Melville Laboratory for Polymer Synthesis, Department of Chemistry, University of Cambridge, Lensfield Road, Cambridge CB2 1EW, United Kingdom

Abstract

Aqueous suspensions of cellulose nanocrystals (CNCs) are known to self-assemble into a chiral nematic liquid crystalline phase, leading to solid-state nanostructured colored films upon solvent evaporation, even in the presence of templating agents. The angular optical response of these structures, and therefore their visual appearance, is completely determined by the spatial arrangement of the CNCs when the drying suspension undergoes a transition from a flowing and liquid crystalline to a kinetically arrested state.

Here, we demonstrate how the angular response of the final film allows for retrieval of key physical properties and the chemical composition of the suspension at the onset of the kinetic arrest, thus capturing a snapshot of the past. To illustrate this methodology, we investigated a dynamically evolving sol-gel co-assembly process by various amounts of organosilica precursor addition, namely 1,2-bis(trimethoxysilyl)ethane (BTMSE). We were able to track the influence of the organosilica condensation on the kinetic arrest and thus explain the angular response of the resulting films. Our *a posteriori* and *in situ* approach is general, it can be applied to a variety of

additives in CNC-based films and it allows accessing key rheological information of the suspension without using any dedicated rheological technique.

Keywords

cellulose nanocrystals; colloidal self-assembly; cholesterics; photonic structures; drying dispersions

Cellulose nanocrystals (CNCs) are sustainable and bio-sourced chiral nano-splinters capable of self-assembling into cholesteric photonic structures by slow drying of colloidal dispersions, offering a sustainable, cost-effective and scalable route to optical materials.^[1–4] Over the past decade, substantial development of CNC-based films with additional functionalities arose from the successful co-assembly of CNCs with other species, e.g., polymers, surfactants, proteins or latexes. Generating hybrid films allowed the community to address the brittleness of pure CNC films but also to incorporate new functionalities (e.g., fluorescence, plasmonic response, etc.).^[5–9] Interestingly, CNC self-assembly is also compatible with several sol-gel precursors such as tetramethyl orthosilicate (TMOS), tetraethyl orthosilicate (TEOS) and organosilica precursors allowing for the fabrication of mesoporous structures inheriting their characteristic chiral photonic properties.^[10–13] The versatility of CNCs and their ability to accommodate these guests allowed for the development of a variety of applications, namely, structural pigments,^[14] anti-counterfeit coatings,^[15] swelling^[16] or mechanochromic sensors,^[17,18] as well as depolarizing^[19] or broadband reflectors.^[20] Importantly, the presence of non-volatile additives often alter significantly the optical properties of the produced films.^[21] In presence of TMOS and related sol-gel precursors, a red-shift in the reflected wavelength is commonly reported and associated to a larger cholesteric pitch, p , but its effect on the orientation of its helical axis, m , remained relatively unexplored.

The self-assembled structure produced upon drying is strongly influenced by the kinetic arrest transition of CNCs that necessarily occurs at some point before a solid material is produced. Before the kinetic arrest transition, the suspension is able to relax and adjust its cholesteric pitch, p (defined as its full-turn periodicity), to the continuously increasing concentration upon solvent evaporation. Once the suspension is kinetically arrested, the pitch is expected to vary mostly as a result of volume decrease and macroscopic contraction along the helix axis, the latter being strongly affected by the cholesteric alignment, the sample geometry and the boundary conditions.^[22–25] This essential step allows for the production of solid-state CNC materials with very distinctive internal structure and corresponding optical properties.^[23,26–29] Only few dedicated studies highlighted the importance of the kinetic arrest in self-assembled CNC systems,^[21,22,30–32] and only few rheological approaches were followed to identify the concentration at which it occurs.^[30] However, the nature of the interaction between CNCs can strongly affect it. Indeed, excessive ionic strength is known to trigger CNC aggregation and lead to a percolated gel.^[30,33,34] Alternatively, very low ionic strength (<0.1 mM) can also cause long-range repulsion even at low volume fraction,^[35] leading to an arrested “colloidal Wigner glass”. This jammed state is characterized by the absence of long range order and the presence of a

finite shear rigidity.^[32,36–39] In these systems, electrostatic caging prevents individual particles from moving independently by hindering each other's motion without being directly in contact.

In this work, we investigate the angular optical response of composite organosilica/Cellulose nanocrystal (OS/CNC) films produced by combining 1,2-bis(trimethoxysilyl)ethane (BTMSE) and CNCs. Various amounts of 1,2-bis(trimethoxysilyl)ethane (BTMSE) were added to an aqueous CNC suspension and the resulting mixtures were cast into petri dishes. The solvent was left to evaporate while the BTMSE was also allowed to condense into organosilica (OS). The optical signature of the kinetic arrest present in the angular response of the dry films allows us to easily capture *a posteriori* the conditions when the suspension underwent kinetic arrest.^[21–23,30,32,40] Such a newly discovered link is highly significant as it enables a better fundamental understanding of the drying kinetic of the colloidal systems, which is challenging to determine otherwise with dedicated rheological techniques.^[30,41]

The initial mass ratio of BTMSE to CNC ($m_{\text{BTMSE}}: m_{\text{CNC}}$) allowed determination of the composition of the final films after the evaporation of water and the condensation of BTMSE into OS. This corresponds, if fully condensed, to a $-\text{CH}_2\text{CH}_2-$ bridged polysilsesquioxane network $(\text{Si}_2\text{O}_3\text{C}_2\text{H}_4)_n$. As we found no significant mismatch between the estimated mass of OS derived from BTMSE:CNC stoichiometry when assuming full condensation and the TGA analysis in a previous study, we have assumed for this work that full condensation occurred in all films.^[42] The estimated volume fractions of OS and CNC in composite films, as well as the resulting optical indices,^[42,43] are reported for convenience in Table 1 and Supporting Information.

Polarized optical microscopy images of the films were observed in reflection and in bright field (Figure 1). Under normal incidence, the films reflect specific colors only in left circular polarization, as expected from their left-handed chiral nematic structure. As previously reported,^[13] the image sequence shows a clear red-shift as more OS is incorporated into the composites. Such a spectral shift has been reported with several other additives and can be understood as a direct effect of the reduction of the vertical collapse of the cholesteric structure upon drying when part of the volatile solvent volume fraction is replaced by a non-volatile counterpart. To quantify the observed redshift as more OS is incorporated, reflection spectra were measured on a large surface area using a double-ended fiber (Figure 1b), which allows for collection of the reflection in a narrow cone of angles along the specular reflection direction.

The angular optical response of the composite films was characterized by angular-resolved optical spectroscopy. In short, each sample is illuminated with white light at a fixed incident angle ($\theta_{\text{in}} = 30^\circ$) and the spectrum of the reflected light is then collected at various angles. The measured intensities are represented as a heat map vs collection angle, θ_{out} , and wavelength, λ , as exemplified in Figure 2a, while the schematic in Figure 2b defines the angles introduced. For each collection angle, the wavelength at the maximum intensity, λ_{peak} , is extracted (Figure 2c), from which several remarkable features can be highlighted. First, the addition of OS leads to a clear redshift of the optical response. Second, for all the samples, a redshift of the reflected wavelength is observed in off-specular conditions (i.e.,

for θ_{in} θ_{out}) with respect to specular (θ_{in} θ_{out}). This is at first counter-intuitive, as a naive application of Bragg's law for a given pitch in the films instead predicts a *blue-shift*. Finally, this tendency to reflect longer wavelength in off-specular conditions decreases significantly as the OS content in the films increases.

These peculiar effects can be explained by the dependence of the pitch on the tilt of the domains. The recorded angular response can be further processed using Bragg's law, corrected by Snell's law at the air-film interface, as introduced by Ferguson for low birefringence cholesterics:^[44]

$$p(\beta) = \lambda_{\text{peak}}(\theta_{in}, \theta_{out}) / [n_{\text{ave}} \cos \psi(\theta_{in}, \theta_{out})] \quad (1)$$

$$\psi(\theta_{in}, \theta_{out}) = \frac{1}{2} \sin^{-1} \left(\frac{\sin \theta_{out}}{n_{\text{ave}}} \right) + \frac{1}{2} \sin^{-1} \left(\frac{\sin \theta_{in}}{n_{\text{ave}}} \right) \quad (2)$$

$$\beta(\theta_{in}, \theta_{out}) = \frac{1}{2} \sin^{-1} \left(\frac{\sin \theta_{out}}{n_{\text{ave}}} \right) - \frac{1}{2} \sin^{-1} \left(\frac{\sin \theta_{in}}{n_{\text{ave}}} \right) \quad (3)$$

where θ_{in} and θ_{out} are the incident and outgoing angles of light, respectively, and n_{ave} is the average optical index of the films. Here we also introduce the local Bragg angle, ψ , and the local tilt, β , of a domain with respect to the vertical axis, both uniquely defined for given (θ_{in} , θ_{out}) conditions. From the data provided by angular-resolved optical spectroscopy, we were able to determine the underlying pitch p and its dependence with the cholesteric domain tilt β , as reported in Figure 2d.

As discussed in recent publications,^[23,32] both the angular response and the pitch vs tilt dependence can be derived from the onset of kinetic arrest occurring in the suspension upon drying. As the kinetic arrest occurs, multiple cholesteric domains are "frozen" in rotation and position, each of them being characterized by a local tilt β_{ka} and a cholesteric pitch p_{ka} , where "ka" refers to the kinetic arrest. Upon further drying, the fixed horizontal boundaries of the dish and the free vertical interface with air lead together to a unidirectional compression of the liquid crystalline structure quantified by a scaling factor $0 < \alpha < 1$. As defined, a value of $\alpha = 0.2$ corresponds to a five-fold compression, (i.e., by a factor $\alpha^{-1} = 5$). The resulting films contain cholesteric domains with different sets of tilts β and pitches p that can be expressed in terms of their initial local tilts β_{ka} and the initial pitch p_{ka} as:

$$p(\beta) = p_{ka} \sqrt{\alpha^2 \cos^2 \beta + \sin^2 \beta} \quad (4)$$

$$\beta = \tan^{-1}[\alpha \tan \beta_{ka}] \quad (5)$$

This mechanism is qualitatively illustrated in Scheme 1. According to this simple model, the tilt β of initially vertically or horizontally aligned domains does not change upon compression ($\beta = \beta_{ka}$) and their associated pitches are respectively the most compressed (i.e., $p(0^\circ) = \alpha p_{ka}$) or not compressed at all (i.e., $p(90^\circ) = p_{ka}$).

The compression of the liquid crystalline structure, characterized by α , can be related to the volume loss occurring between the kinetic arrest and the final film. Since the pitch variation is proportional to the volume contraction, which is occurring predominantly along the vertical direction, the volume fraction $\Phi_{\text{CNC}}^{\text{ka}}$ at the kinetic arrest can be estimated as

$$\Phi_{\text{CNC}}^{\text{ka}} = \alpha \Phi_{\text{CNC}} , \quad (6)$$

where Φ_{CNC} is the volume fraction of CNCs in the final film. In the absence of a non-volatile additive and neglecting the porosity of the CNC films, we can assume here $\Phi_{\text{CNC}} = 1$ in the film and retrieve the expression $\Phi_{\text{CNC}}^{\text{ka}} = \alpha$, introduced in our previous work.^[32] When additional OS is present in the film, equation (6) still holds, except that Φ_{CNC} is now evaluated from the mass ratio $m_{\text{BTMSE}}: m_{\text{CNC}}$ used to prepare the films and reported in Table 1 (details in Supporting Information).

From our knowledge of the films composition (after all relative mass fractions were converted into volume fractions, *cf.* Table 1) and using the data provided by angular-resolved optical spectroscopy, we were able to apply this model and extract two fitting parameters, α and $p(0^\circ)$ (Figure 3a,b), or equivalently, α and p_{ka} (Figure 3a,c). From these values, which were extracted solely from optical analysis, we were able to recover key information about the suspension at the kinetic arrest, such as the volume fraction, the pitch and the concentration of CNCs and additives (Figure 3, more details in Table S1-2).

To validate our approach, we also compared the pitches estimated by our optical analysis with direct SEM observations. According to eq. (4-5), the direct pitch measurement in SEM in vertical domains is expected to match $p(0) = \alpha p_{\text{ka}}$ (Figure 3b), while for those tilted by 90° they should compare with $p(90^\circ) = p_{\text{ka}}$ (Figure 3c and Figure S1). While extremely tilted domains are rare, the measurements made on the few encountered occurrences (on the sample $m_{\text{BTMSE}}: m_{\text{CNC}} = 60:40$) appeared in excellent agreement with the estimations from our optical analysis.

As more OS is incorporated, an overall increase of the pitch $p(0)$ is observed (Figure 3b). Intuitively, this can be easily understood as a direct consequence of the decrease of the vertical compression experienced by the suspension, since a fraction of the initial volatile solvent (in our case, water) has been replaced by the non-volatile OS, reducing the magnitude of the vertical compression. However, the presence of an additive could also interfere with the self-assembly and the chiral interactions between CNCs, either to enhance or reduce them.^[21] Therefore, if the added BTMSE would not modify the twisting between CNCs, we could expect the final pitch $p(0)$ of vertical domains to simply increase as a direct proportion of the added volume fraction of incorporated OS

$$p(0^\circ) = p_{\text{CNC}}(0^\circ) / \Phi_{\text{CNC}} , \quad (7)$$

where $p_{\text{CNC}}(0^\circ)$ is the pitch of vertical domains in the pure CNC film, used here as a reference. This ideal, non-interacting case is represented with a gray dashed line in Figure 3b. The observed pitch values qualitatively follow a similar trend, with a small pitch drift to lower values that will be discussed later.

The estimated CNC concentration at the kinetic arrest, $\Phi_{\text{CNC}}^{\text{ka}}$, appears to increase with addition of BTMSE (Figure 3d) while the pitch at the kinetic arrest, p_{ka} , decreases, and these two effects are amplified for larger $m_{\text{BTMSE}}: m_{\text{CNC}}$ ratios, i.e., initially weak for $\Phi_{\text{OS}} \approx 30\%$ and becoming much stronger at $\Phi_{\text{OS}} \approx 60\%$. These observations suggest that the addition of BTMSE postpones the kinetic arrest. This “fluidifying effect” can be surprising, since sol-gel OS precursors like BTMSE also solidify themselves. Understanding this phenomenon is essential as it strongly affects the angular response of the resulting films. Indeed, the increase of $\Phi_{\text{CNC}}^{\text{ka}}$ combined with the decrease of Φ_{CNC} in the dry film as more OS is incorporated greatly reduces the overall vertical compression, α^{-1} , of the cholesteric structure upon solvent evaporation (Figure 3a). The origin of this dramatic decrease of the vertical compression is better understood with Figure 3f, where the pitch evolution from the kinetic arrest to the dry film is shown as a function of Φ_{CNC} as more OS is incorporated. Since the anisotropic strain causes the red-shift of the off-specular response, it explains why films with more OS present less red-shift in off-specular conditions.

To capture the twisting behavior of CNCs in the arrested suspension state, it is informative to decouple it from their different Φ_{CNC} in the film or $\Phi_{\text{CNC}}^{\text{ka}}$ at their individual kinetic arrest transitions. Upon solvent evaporation, from the onset of the kinetic arrest till complete film collapse, the pitch of vertical domains decreases as $p(0, \Phi_{\text{CNC}}^{\text{susp}}) = p_{\text{ka}} \Phi_{\text{CNC}}^{\text{ka}} / \Phi_{\text{CNC}}^{\text{susp}}$, thus as $\sim 1 / \Phi_{\text{CNC}}^{\text{susp}}$, where $\Phi_{\text{CNC}}^{\text{susp}}$ is the volume fraction of CNC at any point in the arrested state.

The term $p_{\text{ka}} \Phi_{\text{CNC}}^{\text{ka}}$ is uniquely defined for each sample and allows for the visualization of a small pitch decrease induced by the presence of added BTMSE at *fixed* CNC concentration in the arrested suspension (Figure 3e). In other words, these observations indicate an increase of the twisting power of the CNCs in the suspension environment prior to kinetic arrest. Note that this conclusion assumed $\rho_{\text{OS}} = 1.685 \text{ g cm}^{-3}$, based on the work of Wang et al. for non-porous OS.^[45] While it is arguable that the density of OS could vary slightly with experimental conditions and thus be in our case slightly different from Wang et al., our conclusion remains valid even for ρ_{OS} as high as 2.1 g cm^{-1} , which is a safe upper limit.

Significantly, the variations of p_{ka} (Figure 3c), $\Phi_{\text{CNC}}^{\text{ka}}$ (Figure 3d) and $p_{\text{ka}} \Phi_{\text{CNC}}^{\text{ka}}$ (Figure 3e) all show an increasing rate of change upon BTMSE addition, indicating that all these effects become more pronounced as the BTMSE volume fraction is increased.

These variations may originate from a decrease of the repulsive electrostatic interactions, as it is known to occur when, e.g., small quantities of electrolyte are added to an aqueous CNC suspension of low ionic strength. Colloidal suspensions of strongly repulsive particles in a low ionic strength medium can undergo a glass transition when concentrated above a threshold concentration.^[46,47] In such systems, the repulsion range is of the order of the Debye length, κ^{-1} , and inducing a small decrease of κ^{-1} can melt the colloidal glass and shift the glass transition to higher CNC concentrations. In suspensions, κ^{-1} scales as $\sqrt{\epsilon_r / I}$, where ϵ_r is the dielectric constant and I is the ionic strength of the medium. It follows that a drop of κ^{-1} is easily introduced by small addition of electrolyte. Such drop explains the pitch reduction in CNC suspension upon electrolyte addition.^[48,49] However, BTMSE is not

a charged species and should not cause significant variation of I , even at concentrations up to 3 M (Figure 3g). An increase of I either from the introduction of small ionic contaminants or the generation of transient polyvalent charged sol-gel species could be considered, but this option is not consistent with the variation of the changes observed on p_{ka} , Φ_{CNC}^{ka} and $p_{ka} \Phi_{CNC}^{ka}$ as more BTMSE is added: the dependence of κ^{-1} as $1/\sqrt{I}$ would favor an initial large effect that should weaken upon further BTMSE addition, while the inverse trend is observed (i.e., a weak effect that becomes much stronger as more BTMSE is added).

The decrease of κ^{-1} as a result of ϵ_r drop could be a more convincing explanation for these observations. While the addition of BTMSE in the aqueous CNC suspension is initially moderate (<10 wt%), the suspension at the kinetic arrest has lost enough water to make the concentration of BTMSE high enough to significantly affect ϵ_r as a co-solvent. Note, while we found no value for the dielectric constant of BTMSE, we can expect a very low dielectric permittivity (<10) considering the absence of strong dipoles or highly polarizable groups in the molecule. The condensation of BTMSE also releases large quantities of methanol (MeOH) during the condensation process. At the point of kinetic arrest, we ignore what proportion of co-solvent is BTMSE or methanol and what fraction of methanol already evaporated. Nevertheless, assuming full condensation of BTMSE and no methanol evaporation at the kinetic arrest (assumptions noted **) provides an upper bound to estimate the volume fraction of methanol in the sample, $\Phi_{MeOH}^{ka, **}$, and more specifically in the solvent fraction, $\Phi_{MeOH}^{ka, solv, **}$ (Figure 3h, details in Supporting Information). This allows for the estimation of the dielectric constant $\epsilon_r^{**, ka}$ in the resulting solvent, and since the Debye length varies as $\sqrt{\epsilon_r}$, we report $\sqrt{\epsilon_r^{**, ka}}$ in Figure 3i. Clearly, $\sqrt{\epsilon_r^{**, ka}}$ changes very little at small BTMSE:CNC ratios but it varies dramatically at larger ratios. The variation of $\epsilon_r^{**, ka}$ induced by adding the BTMSE is thus more likely what causes the observed variations of p_{ka} , Φ_{CNC}^{ka} and $p_{ka} \Phi_{CNC}^{ka}$ reported in Figure 3. Note that a change of ϵ_r in the suspension can also affect the associated van der Waals interactions between CNCs and additionally modify how CNCs mutually interact at high concentration and their corresponding chiral nematic pitch in solution.^[50]

Alternatively, the condensation of BTMSE into dynamically growing nanoclusters of OS can also be responsible for the decrease of p_{ka} and $p_{ka} \Phi_{CNC}^{ka}$ via a depletion and fractionation effect, whereby a certain fraction of the OS nanoclusters would grow larger and get expelled from the cholesteric domains (into the space between tactoids) and induce a higher local concentration of CNCs in the cholesteric phase. Such fractionation is usually observed for much larger nanoparticles (≥ 50 nm) in biphasic CNC suspensions.^[51–53] This could occur here because of the high volume fraction of OS nanoparticles and their dynamically evolving size distribution as the condensation progresses. A larger number of smaller tactoids could facilitate the pitch equilibration upon concentration and thus postpone the kinetic arrest, effectively increasing Φ_{CNC}^{ka} . Importantly, this phenomenon does not depend on the nature of the kinetic arrest, i.e., whether it evolves into an attractive gel or a repulsive glass. While the optical analysis of the final films in Figure 1a does not easily allow for a reliable estimation of an average “domain size” to compare between samples, the grain boundaries between

domains appear much more pronounced as more OS is added, which could be due to local OS accumulation. Further work is required to validate the proposed scenarios.

To conclude, the angular optical properties of CNC-based photonic films are tightly related to the kinetic arrest transition upon solvent evaporation, and this relationship is important for two reasons. First, the angular optical response can be used to estimate the composition of the suspension undergoing kinetic arrest and this allows decoupling of the effects of any additional species on the self-assembly in a rapid and elegant way. We illustrated this by elucidating the variations of key parameters we introduced, such as p_{ka} , Φ_{CNC}^{ka} and p_{ka} Φ_{CNC}^{ka} , and we found indications that the addition of OS precursor (BTMSE) results in a postponing of the kinetic arrest and a slight reduction of the pitch in suspension *in its arrested state*. The cause could be either a drop of dielectric constant of the solvent with significant release of methanol (associated with a glass transition at the kinetic arrest), or a depletion and fractionation of part of the OS nanoclusters during the condensation. Second, the dependence of the kinetic arrest with additives is shown to control the angular optical response of these systems, through the parameters $p(0)$ and a (or as p_{ka} and a) and justifies paying attention on this transition for the production of CNC-based materials with well-defined photonic properties. Indeed, the angular optical response of the CNC films present a strong red-shift in their off-specular response that is dramatically reduced in the presence of OS. This contributes to reducing the angular dependency of the reflected wavelength (off-specular iridescence). Finally, while the outcomes of this work are directly relevant to the broad community studying CNC-based photonic films and their applications, the experimental simplicity of our approach and the robustness of their conclusions suggest it could be employed as a model system to investigate the onset of kinetic arrest in self-assembling dispersions and its dependence with various experimental parameters.

Experimental Section

General

BTMSE (1,2-bis(trimethoxysilyl)ethane, Acros Organics) was used without further purification. The CNCs were supplied by FPInnovation. The procedure of their preparation is similar to a previous work and is detailed in Supporting Information.^[18]

Preparation of OS/CNC composite films

OS/CNC composite films were prepared by first probe sonicating the CNC suspension, then adding BTMSE dropwise with continuous stirring at room temperature, using the ratios of BTMSE/CNC (cf. Table 1). Films were cast by pouring the mixtures into polystyrene Petri dishes and leaving to dry under ambient conditions (details in Supporting Information).

Sample characterization methods using *polarized optical microscopy* (POM), *spectroscopy*, *angular-resolved optical spectroscopy* with high dynamic range^[23,54,55] and *scanning electron microscopy* (SEM) are detailed in Supporting information.

Supplementary Material

Refer to Web version on PubMed Central for supplementary material.

Acknowledgements

The authors thank Ahu Gümrah Parry for valuable discussions and Richard M. Parker for critical reading of the manuscript. S.V. acknowledges BBSRC David Phillips fellowship [BB/K014617/1], the EPSRC grants [EP/R511675/1, EP/N016920/1, EP/K503757/1], The Isaac Newton Trust Cambridge 1423(g) 76933, European Research Council [ERC-2014-STG H2020 639088, ERC-PoC-2017 790518]. G.G. acknowledges EPSRC [1525292]. M.J.M. thanks NSERC for a Discovery Grant. The authors declare no conflict of interest.

References

- [1]. Moon RJ, Martini A, Nairn J, Simonsen J, Youngblood J. *Chem Soc Rev.* 2011; 40:3941. [PubMed: 21566801]
- [2]. Lagerwall JF, Schütz C, Salajkova M, Noh J, Park J Hyun, Scalia G, Bergström L. *NPG Asia Mater.* 2014; 6:e80.
- [3]. Parker RM, Guidetti G, Williams CA, Zhao T, Narkevicius A, Vignolini S, Frka-Petesic B. *Adv Mater.* 2018; 30
- [4]. Kontturi E, Laaksonen P, Linder MB, Nonappa AH, Gröschel AH, Rojas OJ, Ikkala O. *Adv Mater.* 2018; 30
- [5]. Guidetti G, Atifi S, Vignolini S, Hamad WY. *Adv Mater.* 2016; 28:10042. [PubMed: 27748533]
- [6]. Bardet R, Belgacem N, Bras J. *ACS Appl Mater Interfaces.* 2015; 7:4010. [PubMed: 25552332]
- [7]. Yao K, Meng Q, Bulone V, Zhou Q. *Adv Mater.* 2017; 29
- [8]. Lukach A, Thérien-Aubin H, Querejeta-Fernández A, Pitch N, Chauve G, Méthot M, Bouchard J, Kumacheva E. *Langmuir.* 2015; 31:5033. [PubMed: 25879581]
- [9]. Cheung CY, Giese M, Kelly JA, Hamad WY, MacLachlan MJ. *ACS Macro Lett.* 2013; 2:1016.
- [10]. Kelly JA, Shopsowitz KE, Ahn JM, Hamad WY, MacLachlan MJ. *Langmuir.* 2012; 28:17256. [PubMed: 23186125]
- [11]. Kelly JA, Giese M, Shopsowitz KE, Hamad WY, MacLachlan MJ. *Acc Chem Res.* 2014; 47:1088. [PubMed: 24694253]
- [12]. Shopsowitz KE, Qi H, Hamad WY, MacLachlan MJ. *Nature.* 2010; 468:422. [PubMed: 21085176]
- [13]. Shopsowitz KE, Hamad WY, MacLachlan MJ. *J Am Chem Soc.* 2012; 134:867. [PubMed: 22188398]
- [14]. Bardet R, Roussel F, Coindeau S, Belgacem N, Bras J. *Carbohydr Polym.* 2015; 122:367. [PubMed: 25817681]
- [15]. Zhang YP, Chodavarapu VP, Kirk AG, Andrews MP. *J Nanophotonics.* 2012; 6:63516.
- [16]. Kelly JA, Shukaliak AM, Cheung CY, Shopsowitz KE, Hamad WY, MacLachlan MJ. *Angew Chemie Int Ed.* 2013; 52:8912.
- [17]. Giese M, Khan MK, Hamad WY, MacLachlan MJ. *ACS Macro Lett.* 2013; 2:818.
- [18]. Shopsowitz KE, Kelly JA, Hamad WY, MacLachlan MJ. *Adv Funct Mater.* 2014; 24:327.
- [19]. Hiratani T, Hamad WY, MacLachlan MJ. *Adv Mater.* 2017; 29
- [20]. Cao Y, Hamad WY, MacLachlan MJ. *Adv Opt Mater.* 2018; 6
- [21]. Mu X, Gray DG. *Langmuir.* 2014; 30:9256. [PubMed: 25069681]
- [22]. Parker RM, Frka-Petesic B, Guidetti G, Kamita G, Consani G, Abell C, Vignolini S. *ACS Nano.* 2016; 10:8443. [PubMed: 27564644]
- [23]. Frka-Petesic B, Guidetti G, Kamita G, Vignolini S. *Adv Mater.* 2017; 29
- [24]. Chen Q, Liu P, Nan F, Zhou L, Zhang J. *Biomacromolecules.* 2014; 15:4343. [PubMed: 25300554]

- [25]. Cherpak V, Korolovych VF, Geryak R, Turiv T, Nepal D, Kelly J, Bunning TJ, Lavrentovich OD, Heller WT, Tsukruk VV. *Nano Lett.* 2018
- [26]. Roman M, Gray DG. *Langmuir.* 2005; 21:5555. [PubMed: 15924489]
- [27]. Licen M, Majaron B, Noh J, Schütz C, Bergström L, Lagerwall J, Drevenšek-Olenik I. *Cellulose.* 2016; 23:3601.
- [28]. Park JH, Noh J, Schütz C, Salazar-Alvarez G, Scalia G, Bergström L, Lagerwall JF. *ChemPhysChem.* 2014; 15:1477. [PubMed: 24677344]
- [29]. Zhao TH, Parker RM, Williams CA, Lim KP, Frka-Petesic B, Vignolini S. *Adv Funct Mater.* 2018; 29
- [30]. Honorato-Rios C, Kuhnhold A, Bruckner JR, Dannert R, Schilling T, Lagerwall JF. *Front Mater.* 2016; 3:21.
- [31]. Gray DG. *Nanomaterials.* 2016; 6:213.
- [32]. Frka-Petesic B, Kamita G, Guidetti G, Vignolini S. *Phys Rev Mater.* 2019; 3
- [33]. Peddireddy KR, Capron I, Nicolai T, Benyahia L. *Biomacromolecules.* 2016; 17:3298. [PubMed: 27584941]
- [34]. Cherhal F, Cousin F, Capron I. *Langmuir.* 2015; 31:5596. [PubMed: 25918887]
- [35]. Araki J, Kuga S. *Langmuir.* 2001; 17:4493.
- [36]. Lindsay HM, Chaikin PM. *J Chem Phys.* 1982; 76:3774.
- [37]. Tanaka H, Meunier J, Bonn D. *Phys Rev E - Stat Nonlinear, Soft Matter Phys.* 2004; 69
- [38]. Tanaka H, Jabbari-Farouji S, Meunier J, Bonn D. *Phys Rev E - Stat Nonlinear, Soft Matter Phys.* 2005; 71
- [39]. Bonn D, Tanaka H, Wegdam G, Kellay H, Meunier J. *Europhys Lett.* 2007; 45:52.
- [40]. Gray DG. *Philos Trans R Soc A Math Phys Eng Sci.* 2018; 376
- [41]. Honorato-Rios C, Lehr C, Schütz C, Sanctuary R, Osipov MA, Baller J, Lagerwall JF. *NPG Asia Mater.* 2018; 10:455.
- [42]. Wang W, Grozea D, Kohli S, Perovic DD, Ozin GA. *ACS Nano.* 2011; 5:1267. [PubMed: 21204583]
- [43]. Dumanli AG, van der Kooij HM, Kamita G, Reisner E, Baumberg JJ, Steiner U, Vignolini S. *ACS Appl Mater Interfaces.* 2014; 6:12302. [PubMed: 25007291]
- [44]. Ferguson JL. *Mol Cryst.* 1966; 1:293.
- [45]. Santos AM, Vasconcelos WL. *Mater Res.* 1999; 2:201.
- [46]. Schlesinger M, Hamad WY, MacLachlan MJ. *Soft Matter.* 2015; 11:4686. [PubMed: 25972020]
- [47]. Zaccarelli E. *J Phys Cond Mat.* 2007; 19
- [48]. Revol J-F, Godbout DL, Gray DG. *J pulp Pap Sci.* 1998; 24:146.
- [49]. Dong XM, Kimura T, Revol J-F, Gray DG. *Langmuir.* 1996; 12:2076.
- [50]. Bruckner JR, Kuhnhold A, Honorato-Rios C, Schilling T, Lagerwall JF. *Langmuir.* 2016; 32:9854. [PubMed: 27571039]
- [51]. Li Y, Suen J Jun-Yan, Prince E, Larin EM, Klinkova A, Thérien-Aubin H, Zhu S, Yang B, Helmy AS, Lavrentovich OD, Kumacheva E. *Nat Commun.* 2016; 7
- [52]. Li Y, Prince E, Cho S, Salari A, Mosaddeghian Golestani Y, Lavrentovich OD, Kumacheva E. *Proc Natl Acad Sci U S A.* 2017; 114:2137. [PubMed: 28193865]
- [53]. Wang P, Hamad WY, MacLachlan MJ. *Angew Chemie Int Ed.* 2018; 57:3360.
- [54]. Kamita G, Frka-Petesic B, Allard A, Dargaud M, King K, Dumanli AAG, Vignolini S. *Adv Opt Mater.* 2016; 4:1950.
- [55]. Song D-P, Jacucci G, Dundar F, Naik A, Fei H-F, Vignolini S, Watkins JJ. *Macromolecules.* 2018; 51:2395. [PubMed: 29681653]

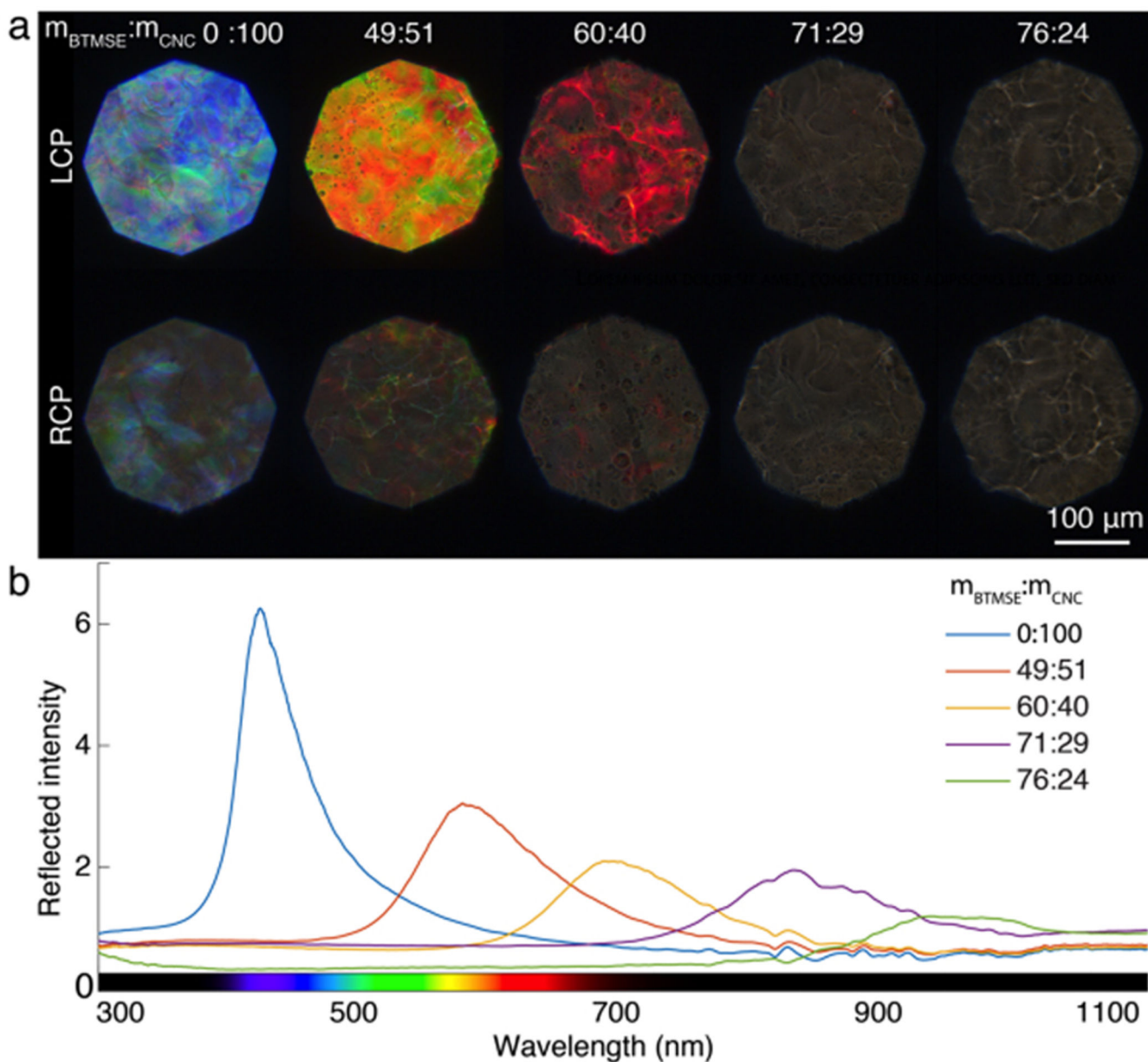


Figure 1. Optical characterization of the composite organosilica/cellulose nanocrystal (OS/CNC) films made with increasing BTMSE:CNC ratios. a) Polarized optical microscopy in reflection using respectively left- (LCP) and right-circular polarization (RCP) filters, showing a red-shift of the reflected light. b) Reflection spectra measured on the same samples using a double-ended fiber in normal incidence, normalized to a white diffuser.

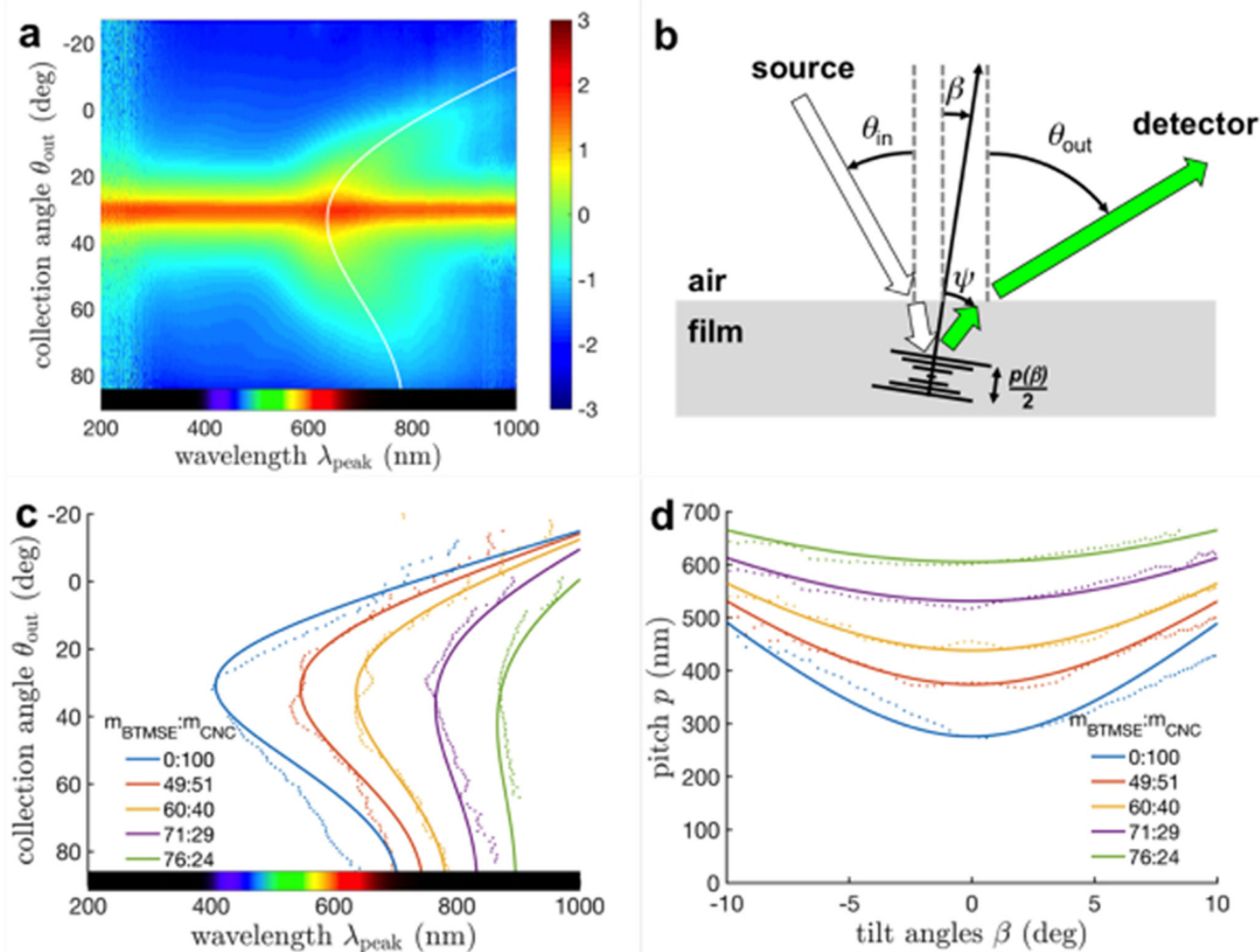
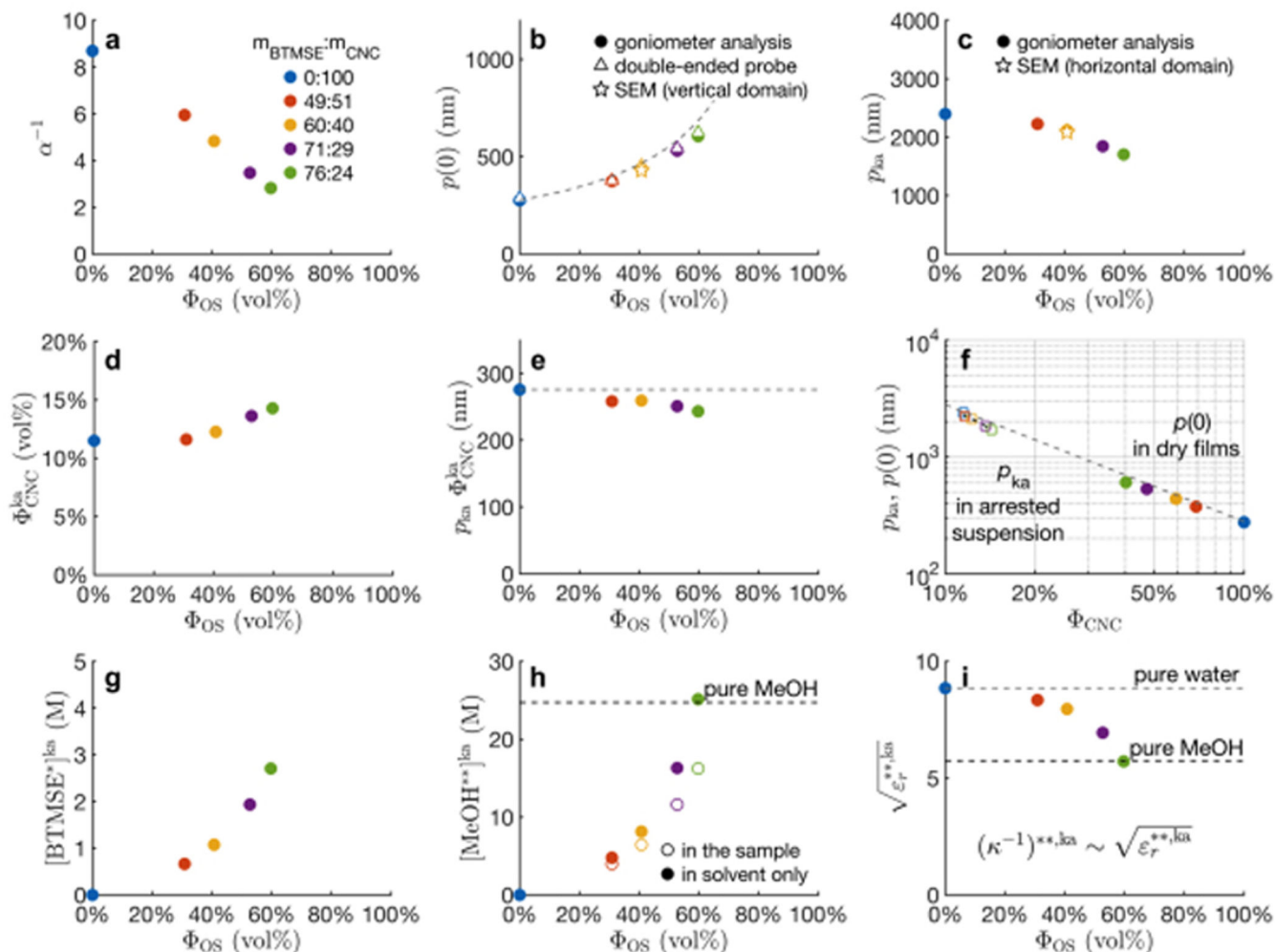


Figure 2.

a) Angular-resolved optical spectroscopy of an OS/CNC composite film ($m_{BTMSE} : m_{CNC} = 60:40$) reporting the light intensity as a heatmap vs collection angles θ_{out} and wavelengths λ and a fit (solid line, using Equations 1-5 and $\theta_{in} = 30^\circ$). b) Schematic of the goniometer set-up and the angle definition. c) Peak wavelength λ_{peak} reflected at different θ_{out} (data in dots, fits in solid lines) and d) the corresponding pitches.

**Figure 3.**

Summary of the information retrieved from the optical analysis of films for different $m_{BTMSE}:m_{CNC}$, and reported in function of volume fractions of OS (Φ_{OS}) or CNC (Φ_{CNC}). α^{-1} : vertical compression factor; $p(\beta)$: pitch of domains of tilt β in films; p_{ka} : pitch at the kinetic arrest, Φ_{CNC}^{ka} : volume fraction at kinetic arrest; $[BTMSE^*]^{ka}$: BTMSE at the kinetic arrest, assuming no condensation has yet occurred; $[MeOH^{**}]^{ka}$, ϵ_r^{**ka} and $(\kappa^{-1})^{**ka}$: maximum MeOH, dielectric constant and Debye length at the kinetic arrest, assuming all the BTMSE has condensed and no MeOH has evaporated yet. The gray dashed lines represent the ideal case for which BTMSE and water would have the same effect on the CNC pitch.

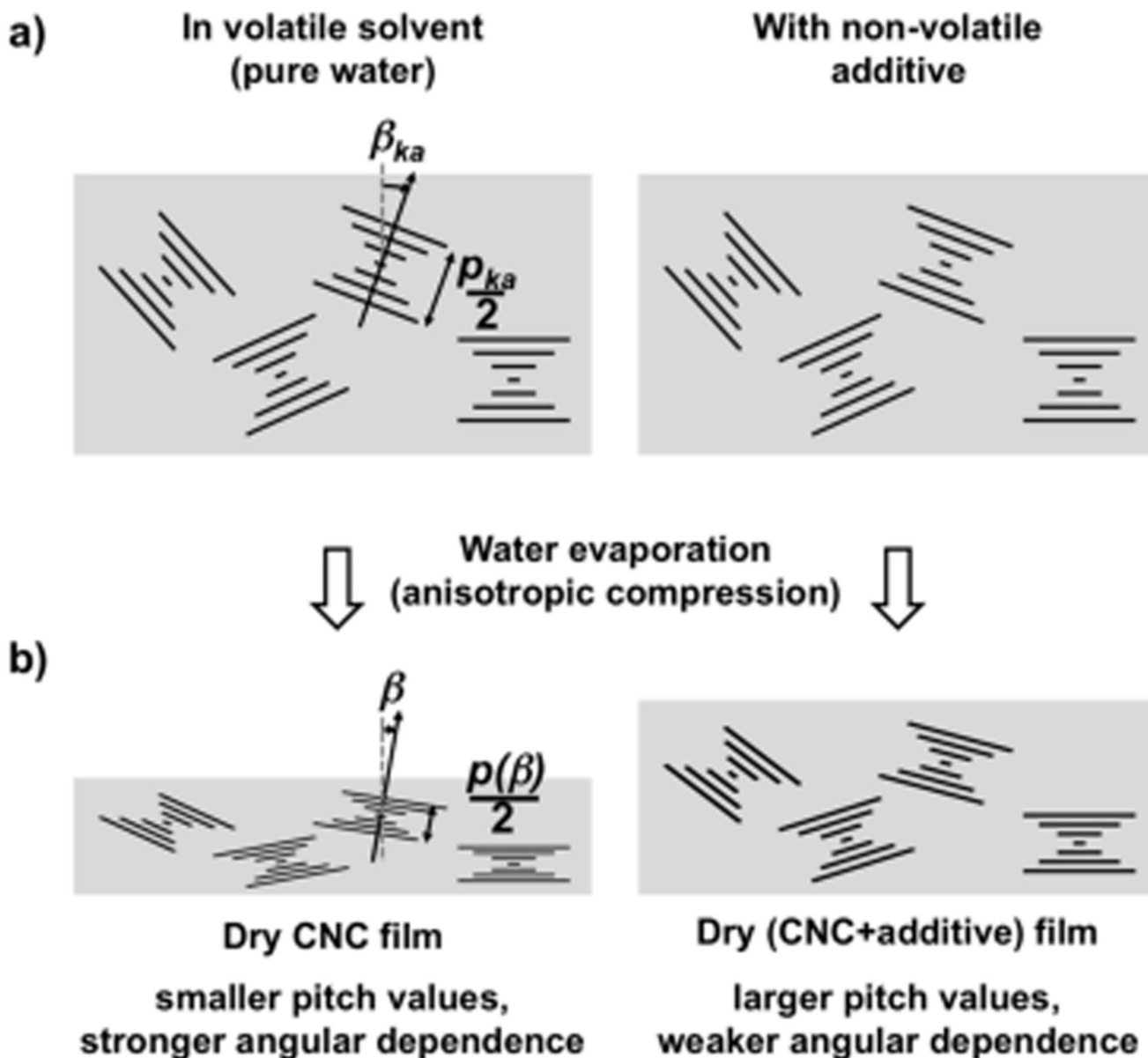
**Scheme 1.**

Illustration of the vertical compression experienced by the cholesteric domains upon solvent compression, in the absence (left) or presence of a non-volatile additive (right), from a) the kinetic arrest transition until b) complete evaporation of the volatile fraction. The final pitch $p(\beta)$ retains information about the initial pitch p_{ka} and its compression ratio α , related to the suspension composition at the kinetic arrest.

Table 1
Summary of the composite film composition.

$m_{\text{BTMSE}}: m_{\text{CNC}}$ [wt/wt]	$[\text{BTMSE}]_{3\text{wt}\%}$ [M] ^{a)}	c_{os} [wt%]	c_{CNC} [wt%]	Φ_{os} [vol%]	Φ_{CNC} [vol%]	n_{ave}
0:100	0.00	0	100	0.0	100.0	1.55(5)
49:51	0.11	32	68	30.9	69.1	1.54(1)
60:40	0.17	42	58	40.7	59.3	1.53(7)
71:29	0.27	54	46	52.7	47.3	1.53(1)
76:24	0.36	61	39	59.8	40.2	1.52(8)

^{a)} $[\text{BTMSE}]_{3\text{wt}\%}$ corresponds to the initial [BTMSE] rescaled to a $c_{\text{CNC}} = 3$ wt% suspension.